

REPORT

 OPEN ACCESS

## Antibody production using a ciliate generates unusual antibody glycoforms displaying enhanced cell-killing activity

Jenny Calow<sup>a,\*</sup>, Anna-Janina Behrens<sup>b,\*</sup>, Sonja Mader<sup>b</sup>, Ulrike Bockau<sup>a</sup>, Weston B. Struwe<sup>b</sup>, David J. Harvey<sup>b</sup>, Kai U. Cormann<sup>c</sup>, Marc M. Nowaczyk<sup>c</sup>, Karin Loser<sup>d</sup>, Daniel Schinor<sup>e</sup>, Marcus W.W. Hartmann<sup>a</sup>, and Max Crispin<sup>b</sup>

<sup>a</sup>Cilian AG, Münster, Germany; <sup>b</sup>Oxford Glycobiology Institute, Department of Biochemistry, University of Oxford, Oxford, UK; <sup>c</sup>Plant Biochemistry, Ruhr University Bochum, Bochum, Germany; <sup>d</sup>Department of Dermatology, University of Münster, Münster, Germany; <sup>e</sup>Wessling GmbH, Pharmaanalytik Münster, Münster, Germany

### ABSTRACT

Antibody glycosylation is a key parameter in the optimization of antibody therapeutics. Here, we describe the production of the anti-cancer monoclonal antibody rituximab in the unicellular ciliate, *Tetrahymena thermophila*. The resulting antibody demonstrated enhanced antibody-dependent cell-mediated cytotoxicity, which we attribute to unusual N-linked glycosylation. Detailed chromatographic and mass spectrometric analysis revealed afucosylated, oligomannose-type glycans, which, as a whole, displayed isomeric structures that deviate from the typical human counterparts, but whose branches were equivalent to fragments of metabolic intermediates observed in human glycoproteins. From the analysis of deposited crystal structures, we predict that the ciliate glycans adopt protein-carbohydrate interactions with the Fc domain that closely mimic those of native complex-type glycans. In addition, terminal glucose structures were identified that match biosynthetic precursors of human glycosylation. Our results suggest that ciliate-based expression systems offer a route to large-scale production of monoclonal antibodies exhibiting glycosylation that imparts enhanced cell killing activity.

**Abbreviations:** mAb, monoclonal antibody; ADCC, antibody-dependent cell-mediated cytotoxicity; CE, capillary electrophoresis; CEX, cation exchange; CID, collision-induced dissociation; DSA-FACE, DNA sequencer-assisted fluorophore assisted carbohydrate electrophoresis; endoA, *Arthrobacter endoglycosidase*; HILIC-UPLC, Hydrophilic interaction chromatography-Ultra performance liquid chromatography; IM ESI-MS, ion mobility electrospray mass spectrometry; PBMC, peripheral blood mononuclear cells; SDS PAGE, sodium dodecyl sulfate polyacrylamide gel electrophoreses; SPR, surface plasmon resonance; *Tt*, *Tetrahymena thermophila*

### ARTICLE HISTORY

Received 15 June 2016  
Revised 10 August 2016  
Accepted 19 August 2016

### KEYWORDS

ADCC; ciliate; monoclonal antibody; N-glycosylation pattern; recombinant expression; rituximab

## Introduction


The freshwater ciliated protozoan *Tetrahymena thermophila* is a very well-characterized unicellular eukaryotic organism.<sup>1</sup> Although ciliates have been extensively used as a model system in molecular and cell biology, their application within the biopharmaceutical industry remains underexplored despite several potential advantages.<sup>2</sup> For example, *T. thermophila* grows rapidly to high cell densities of about  $5 \times 10^6$  cells/mL in inexpensive cell culture media, requiring only simple up-scalable bioreactors comparable to those used for yeast and *Escherichia coli* fermentation if used for biopharmaceutical production.<sup>3</sup> In addition, it is regarded to be a biologically safe organism thought to be free from human pathogens, as there is generally no evidence that it harbours any pathogenic viruses or pyrogens.<sup>4</sup> The availability and annotation of non-germline macronucleus genome sequences provided the basis for the development of molecular methods specifically designed to genetically modify its genome.<sup>5–11</sup> Hence, numerous homo- and heterologous proteins have already been successfully and stably expressed in *T. thermophila*.<sup>2,4,12–14</sup>

*T. thermophila* is thus a beneficial expression system with the potential to offer significant advantages in the production of high quality proteins and glycoproteins.

Recombinant monoclonal antibodies (mAbs) constitute the majority of marketed biopharmaceuticals, and they are used to treat a wide range of diseases, particularly include cancer, but also infectious and inflammatory diseases.<sup>15</sup> The clinical success of mAbs is based on their high target antigen specificity and the fragment crystallizable (Fc)-associated effector functions. The latter can either result from the formation of immune complexes formed after association with Fc receptors on immune effector cells (e.g., monocytes, natural killer cells, macrophages and dendritic cells) or from activating the classical complement system via binding of the C1 complex.<sup>16</sup> Antibody receptor recognition is strongly influenced by the type of N-glycan linked to the conserved Asn<sup>297</sup> residues on both C $\gamma$ 2 domains.<sup>17</sup> The glycosylation pattern is determined by the expression system's glycosylation machinery and can be highly heterogeneous, with each glycoform exhibiting particular physical and biological properties.

**CONTACT** Jenny Calow  [calow@cilian.de](mailto:calow@cilian.de)

\*These authors share first co-authorship.

 Supplemental data for this article can be accessed on the [publisher's website](#).

Published with license by Taylor & Francis Group, LLC © 2016 Cilian AG

This is an Open Access article distributed under the terms of the Creative Commons Attribution-Non-Commercial License (<http://creativecommons.org/licenses/by-nc/3.0/>), which permits unrestricted non-commercial use, distribution, and reproduction in any medium, provided the original work is properly cited. The moral rights of the named author(s) have been asserted.

Comparing antibody biogenesis across the range of eukaryotic systems explored by the biopharmaceutical industry, we observe that the early protein folding and glycosylation processes are highly conserved. However, diversification of glycoforms, predominantly in the Golgi apparatus, is shaped through the opposing influences of protein-directed control of glycosylation and cell-specific remodelling of glycans.<sup>18</sup> Different recombinant production systems provide highly individual posttranslational modifications to the proteins. One of the most important of these modifications is N-glycosylation, which has great influence on antibody effector functions, pharmacokinetic properties, thermodynamic stability, safety and efficacy.<sup>19,20</sup>

Given the range of effector function properties made accessible by the isolation of different antibody glycoforms, even rare or moderately low abundant glycoforms are being investigated for their biopharmaceutical application. For example, highly sialylated antibodies show anti-inflammatory properties, while oligomannose-type and afucosylated glycoforms enhance FcγRIIIa binding and elevate antibody-dependent cell-mediated cytotoxicity (ADCC).<sup>21–24</sup> Importantly, following the approval of the afucosylated antibody mogamulizumab, such glycan-engineered antibodies are now benefiting patients.<sup>25</sup>

Almost all commercially available mAbs are currently produced by mammalian cell lines, mainly due to the human-like glycosylation profile and the thus largely avoided immunogenic reactions against the therapeutic antibody. Many efforts have been undertaken to produce antibodies in alternative production systems like lepidopteran cells, yeast, transgenic animals and plants in order to lower the cost of production.<sup>26–29</sup> None of these production systems has gained significant commercial attention yet likely, in part, due to the differences in their N-linked glycosylation compared to humans. However, glyco-engineering platforms, such as Potelligent<sup>®30</sup> and GlycoMab<sup>®31</sup> for mammalian cell lines or GlycoFi<sup>®32</sup> for the yeast expression system *Pichia pastoris*, were developed to improve the efficacy of mAbs. Some of these antibodies are currently in clinical studies.<sup>25</sup> In consequence, very high demands are placed on new expression systems for the production of mAbs. The yields must be high, costs controlled, and the resulting product must be of high quality, including displaying optimal N-linked glycosylation that is synchronized to the required biological effector function.

Wildtype *T. thermophila* cells transformed to express and secrete high levels of proteins with therapeutic or nutraceutical potential generally exhibit typical, eukaryotic-like posttranslational modifications with one notable exception, N-linked glycosylation. Detailed analyses of the N-linked glycosylation of *T. thermophila* are currently lacking, although a study of the recombinantly expressed and secreted DNase I utilizing DNA sequencer-assisted fluorophore assisted carbohydrate electrophoresis (DSA-FACE) identified mainly paucimannose and oligomannose-type N-linked glycans (Man<sub>2–5</sub>GlcNAc<sub>2</sub>).<sup>14</sup> Furthermore, we are not aware of any scientific reports describing the recombinant expression of a mAb in *T. thermophila*.

Here, we report the expression in *T. thermophila* of a chimeric human-mouse monoclonal anti-CD20 antibody that exhibits comparable antigen binding properties and

similar apoptosis induction abilities in target cells compared to the commercial anti-CD20 antibody produced in Chinese hamster ovary (CHO) cells (rituximab, MabThera<sup>®</sup>, Roche). Our anti-CD20 antibody expressed in *T. thermophila* displays a higher affinity to the Fc receptor FcγRIIIA and exhibits stronger ADCC. We furthermore provide a detailed study of the N-glycosylation profile exhibited by *T. thermophila*. The ciliate produces afucosylated, oligomannose-type, as well as glucose-terminated N-linked glycans. We attribute the observed enhanced effector functions to this unusual N-linked glycosylation profile. We show that the glycoforms resemble different arms of naturally occurring human glycans, and we rationalize the effector properties of the Fc glycoforms using a combination of existing crystal structures.

## Results

### Recombinant production of anti-CD20 mAb with *T. thermophila*

In order to express the full-length monoclonal anti-CD20 antibody (rituximab, clone C2B8) in ciliates, we used codon-optimized artificial genes, according to the codon bias for highly expressed genes in *T. thermophila*.<sup>33,34</sup> Full-length cDNA for the heavy chain (HC) and light chain (LC) of the antibody were cloned into the rDNA ori-based pAX vector derivative and into a pKOIX-based integrative expression vector variant, respectively (Fig. 1A).<sup>9</sup> Conjugating *T. thermophila* wildtype cells were consecutively transformed with both vectors. Resulting transformants were screened for levels of expression and secretion of the anti-CD20 antibody by ELISA. Heavy and light chain double transformants displaying the highest antibody secretion were selected for future work.

In initial experiments, cell densities of  $3.5 \times 10^6$  cells/mL and yields of 20 mg/L/day could be reached using lab-scale batch fermentation. In order to characterize the anti-CD20 expressed by *T. thermophila* (from here on referred to as *Tt/C2B8*), we purified the mAb from cell culture supernatant by Protein A affinity chromatography (Fig. 1). Supernatant, flow through fraction and eluate fraction were analyzed by silver staining and western blot subsequent to sodium dodecyl sulfate polyacrylamide gel electrophoresis (SDS-PAGE) (Fig. 1B,C). The full IgG band of *Tt/C2B8* in the supernatant and in the eluate has a comparable size to the commercial MabThera<sup>®</sup> full IgG band, which indicates correct expression, assembly and secretion of the antibody. The bands at about 50 kDa (HC) and about 25 kDa (LC) were only visible in the immunoblot analysis (Fig. 1C), not in the silver stained gel (Fig. 1B), and represent small amounts of non-assembled antibody fragments.

The western blot analysis (Fig. 1C) reveals 2 HC bands, suggesting 2 different N-glycosylation variants. To further investigate this and to improve the resolution, we analyzed the sample using a Bioanalyzer 2100 (Fig. 1D). Treatment with PNGase F (peptide N-glycosidase F) led to aglycosylated HCs with similar apparent molecular weights for the commercial MabThera<sup>®</sup> and for *Tt/C2B8*. Under reducing conditions, we observed a double band for the HC of the *Tt/C2B8*. The upper band corresponds to the

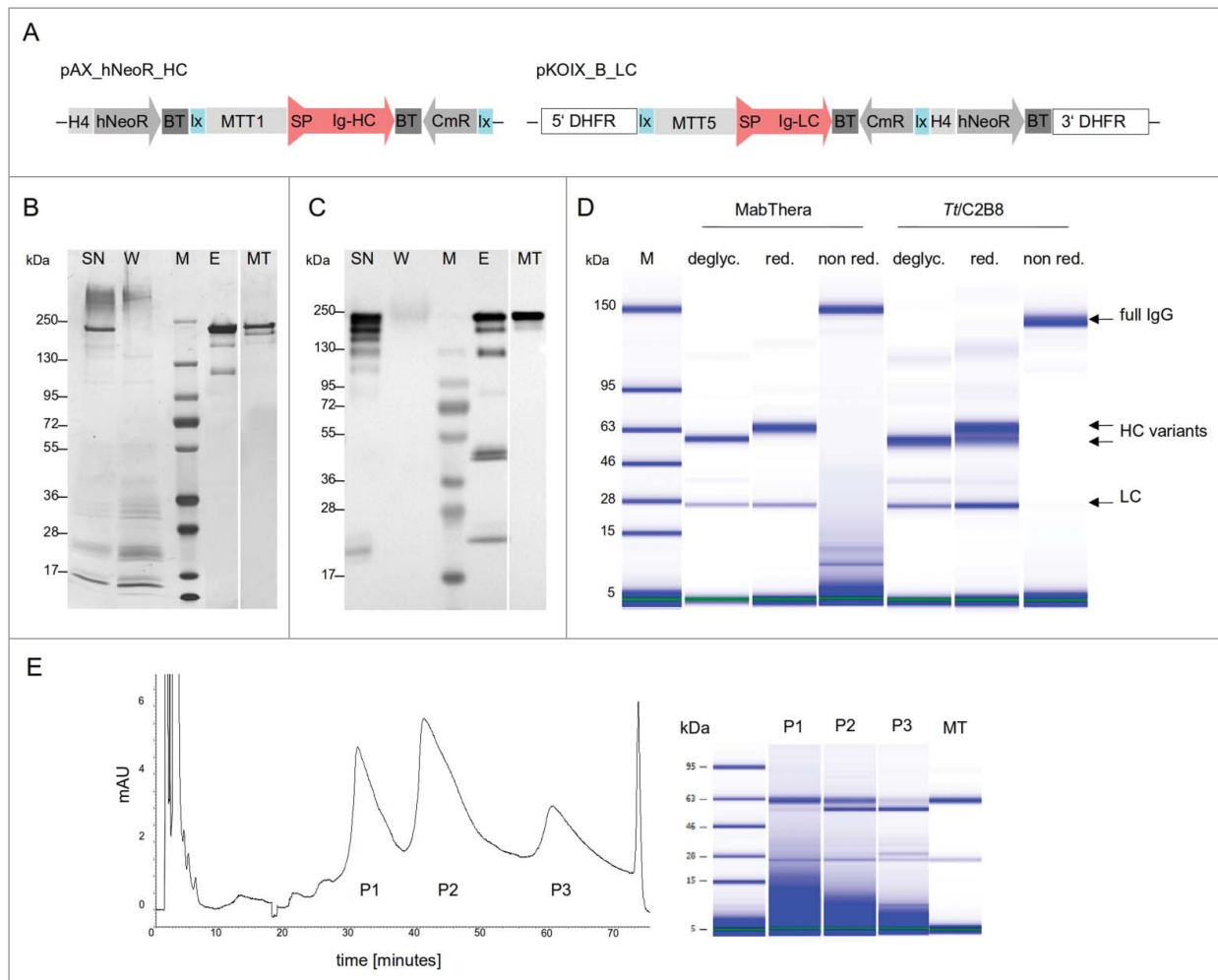


**Figure 1.** Expression, purification and glycoform separation of anti-CD20 antibody expressed by *T. thermophila*. (A) Two different expression cassettes in 2 different vectors were used to generate transgenic *T. thermophila* strains. The pAX\_hNeoR\_HC plasmid contains the full length cDNA encoding the heavy chain of anti-CD20, fused to the signal sequence of Tetrahymena PGP1 (signal peptide, amino acids 1–18), flanked by a ~1 kb MTT1 promoter active sequence and the BTU2 terminator (~350bp). The pKOIX\_B\_LC plasmid contains the full length cDNA encoding the light chain gene of anti-CD20, fused to the signal sequence of Tetrahymena PGP1 (signal peptide, amino acids 1–18), controlled by a ~1.2 kb MTT5 promoter active sequence and the BTU2 terminator (~350 bp). The whole expression cassette is flanked by DHFR-TS 3' and 5' integration sequences (each ~1.5 kb). Ix, lox promoter cassette; CmR, chloramphenicol resistance cassette, H4, Histon promoter, Ig-HC, immunoglobulin heavy chain, Ig-LC, immunoglobulin light chain, DHFR, Dihydrofolatreductase, BsdR, blasticidin resistance cassette, hNeoR, neomycin resistance cassette, BT,  $\beta$  tubulin terminator sequence. (B–D) Tetrahymena anti-CD20 antibody was purified from cadmium-induced cell culture supernatant using Protein A affinity chromatography. Supernatant (SN), flow-through fraction (W) and eluate fraction (E) were analyzed by SDS-PAGE and silver staining (B) and immune blot using HRP conjugated anti-human IgG antibody (C). Full IgG band of *Tt/C2B8* was compared to MabThera (MT) full IgG band. Purified *Tt/C2B8* and MabThera<sup>®</sup> were analyzed regarding their N-linked glycan occupancy using Bioanalyzer 2100. Antibody samples were deglycosylated by PNGaseF treatment (deglyc.) and separated under reduced (red.) and nonreduced (non red.) conditions (D). M, prestained standard. (E) Chromatogram of a representative HPLC - CEX resulting in separation of anti-CD20 antibody variants differing in heavy chain N-linked glycan occupancy. A gradient of salt at pH 4.0 was used for elution. Antibody samples from separated peaks (P1 – P3) were analyzed using Bioanalyzer 2100 (P1, 99% glycosylated HC; P2 51% glycosylated HC; P3 24% glycosylated HC, MT, MabThera<sup>®</sup>).

glycosylated HC band of MabThera<sup>®</sup>. The band at the lower molecular weight indicates an aglycosylated portion of the produced HCs.

To confirm the presence of *Tt/C2B8* glycosylation variants and to precisely determine its molecular weight, we measured the intact antibody by high-resolution native mass spectrometry (Fig. 2; amino acids sequence in Supplementary Information). Three distinct species were identified corresponding to aglycosylated, mono-glycosylated and di-glycosylated antibody. Glycan structures, confirmed by ion mobility mass spectrometry (discussed below), were identified within each glycosylated variant. A truncated form of the aglycosylated antibody was also identified consistent with lysine clipping on the HC C-terminus, although this was a minor ion. Following PNGase

F treatment, only the aglycosylated species were present, confirming the identification of N-glycosylation of the mono- and di-glycosylated *Tt/C2B8* variants.

### Characterization of the binding ability of anti-CD20 antibody expressed by *T. thermophila*

We then aimed to compare the binding abilities of the recombinantly produced *Tt/C2B8* and MabThera<sup>®</sup> to their CD20 epitope expressed on human B cells. Hence, freshly isolated peripheral blood mononuclear cells (PBMC) were incubated either with MabThera<sup>®</sup> or *Tt/C2B8* and subsequently analyzed by flow cytometry (Fig. 3A). The *Tt/C2B8* recognizes the CD20 epitopes on human B cells in

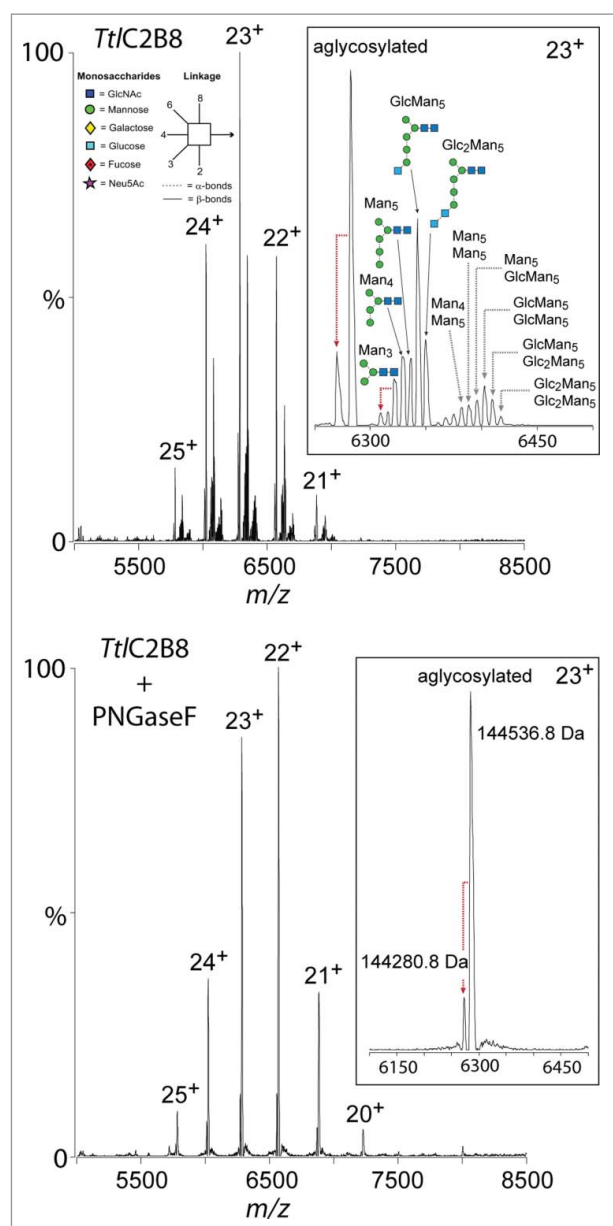


**Figure 2.** Native mass spectrometry of glycosylated and PNGase F treated *Tt/C2B8*. Intact mass spectrum reveals aglycosylated, mono-glycosylated and di-glycosylated variants (top). The analyzed *Tt/C2B8* was purified by Protein A chromatography (Fig. 1D). Detailed analysis of a single charge state ( $23^+$ ) identifies N-glycan compositions on each heavy chain. PNGase F treated *Tt/C2B8* (bottom spectrum) confirms N-glycan compositions and also indicates C-terminal lysine clipping of the heavy chain. The glycans have been assigned to structures based on the glycan analysis presented in Figs. 4 and 5. Glycan structures are displayed as shown in the legend on the top left with symbols and linkages as proposed by Harvey *et al.*<sup>75</sup> using the color scheme adopted by the Consortium for Functional Glycomics.

the same manner as the MabThera<sup>®</sup>. The induction of apoptosis in human B cells is a well-described biological effector function of the anti-CD20 antibody.<sup>35</sup> We thus incubated PBMCs again with both antibodies and used the apoptotic marker Annexin V afterwards for cell staining. Additionally, the cells were counterstained with the live/dead marker propidium iodide and analyzed using flow cytometry. The cells were gated for CD19/CD20 positive B cells. *Tt/C2B8* as well as MabThera<sup>®</sup> were able to induce apoptosis in about 45 - 54% (Fig. 3B) of the human B cells.

### Binding affinity to *FcγRIIIA* receptor variants

Binding of the Fc region of the anti-CD20 antibody to *FcγRIIIA* receptor is important for elicitation of biochemical effector functions of mAbs, such as ADCC.<sup>36</sup> To assess the binding affinity, we employed surface plasmon resonance (SPR) analysis using a recombinant extracellular domain of human CD16. Due to a polymorphism for *FcγRIIIA* in humans, both receptor variants 176 Val (F) and 176 Phe (V) were analyzed. Sensorgrams of the interactions of both *FcγRIIIA* variants and MabThera<sup>®</sup> or anti-CD20 expressed by *T. thermophila* are shown in Fig. 3C. In contrast to the dissociation rate constant  $k_d$ , which shows minor differences between MabThera<sup>®</sup> and *Tt/C2B8* for a given *FcγRIIIA* variant, the association rate constant  $k_a$  of *Tt/C2B8* is  $\sim 4$  to 5 times higher than that of MabThera<sup>®</sup>. Accordingly, the dissociation constant ( $K_D$ ) was more than 5 times lower (Fig. 3C), indicating an enhanced affinity of *Tt/C2B8* to the *FcγRIIIA* compared to MabThera<sup>®</sup>.

As mentioned above, *T. thermophila* produces a population of aglycosylated HCs (Fig. 1D) leading to the formation of  $\alpha$ -, hemi- and fully glycosylated full IgG. We successfully separated the fully glycosylated IgG fraction by cation-exchange HPLC (CEX-HPLC, Fig. 1E). This is of particular importance because even hemiglycosylated antibodies have been described to have lower *Fcγ* - receptor affinities, and hence decreased ADCC efficacy.<sup>37</sup>

### *T. thermophila*-expressed anti-CD20 displays a higher ADCC

It is thought that ADCC contributes substantially to the *in vivo* antitumor activity of IgG1 antibodies.<sup>38,39</sup> As the *Tt/C2B8* exhibits a significantly higher affinity to the *FcγRIIIA* receptor, we hypothesized that this would also result in a higher ADCC effector function. To demonstrate this, an ADCC reporter bioassay was performed using the fully glycosylated antibody preparation after CEX-HPLC separation (Fig. 1E). In the ADCC reporter assay, classical effector cells, e.g., natural killer cells, are replaced by engineered Jurkat cells stably expressing the *FcγRIIIA* receptor and an NFAT (Nuclear factor of activated T-cells) response element driving the expression of a firefly luciferase.<sup>40</sup> After the successful cross-linking of the CD20-positive Raji cells and the Jurkat cells with the anti-CD20 antibodies, luminescence readout was quantified as an early result of ADCC mechanism of action. Cultivation of Raji and Jurkat/*FcγRIIIA*/NFAT cells with *Tt/C2B8* led to a 17 times stronger ( $EC_{50}$  7 ng/mL, half maximal effective concentration) dose-dependent activation of the *Fcγ*-receptor compared to MabThera<sup>®</sup> ( $EC_{50}$  123 ng/mL; Fig. 3D).

### Glycosylation analysis

As the higher ADCC of *Tt/C2B8* can most likely be explained by the glycans present on the conserved Asn<sup>297</sup> of the HC, we performed glycan analysis by ion mobility electrospray mass spectrometry (IM ESI-MS) and HILIC-UPLC. IM ESI-MS analysis revealed the presence of 6 different glycans present on *Tt/C2B8* (Fig. 4). The oligomannose-type glycans  $Man_{3-5}GlcNAc_2$  were detected, as well as the glucose-terminated structures

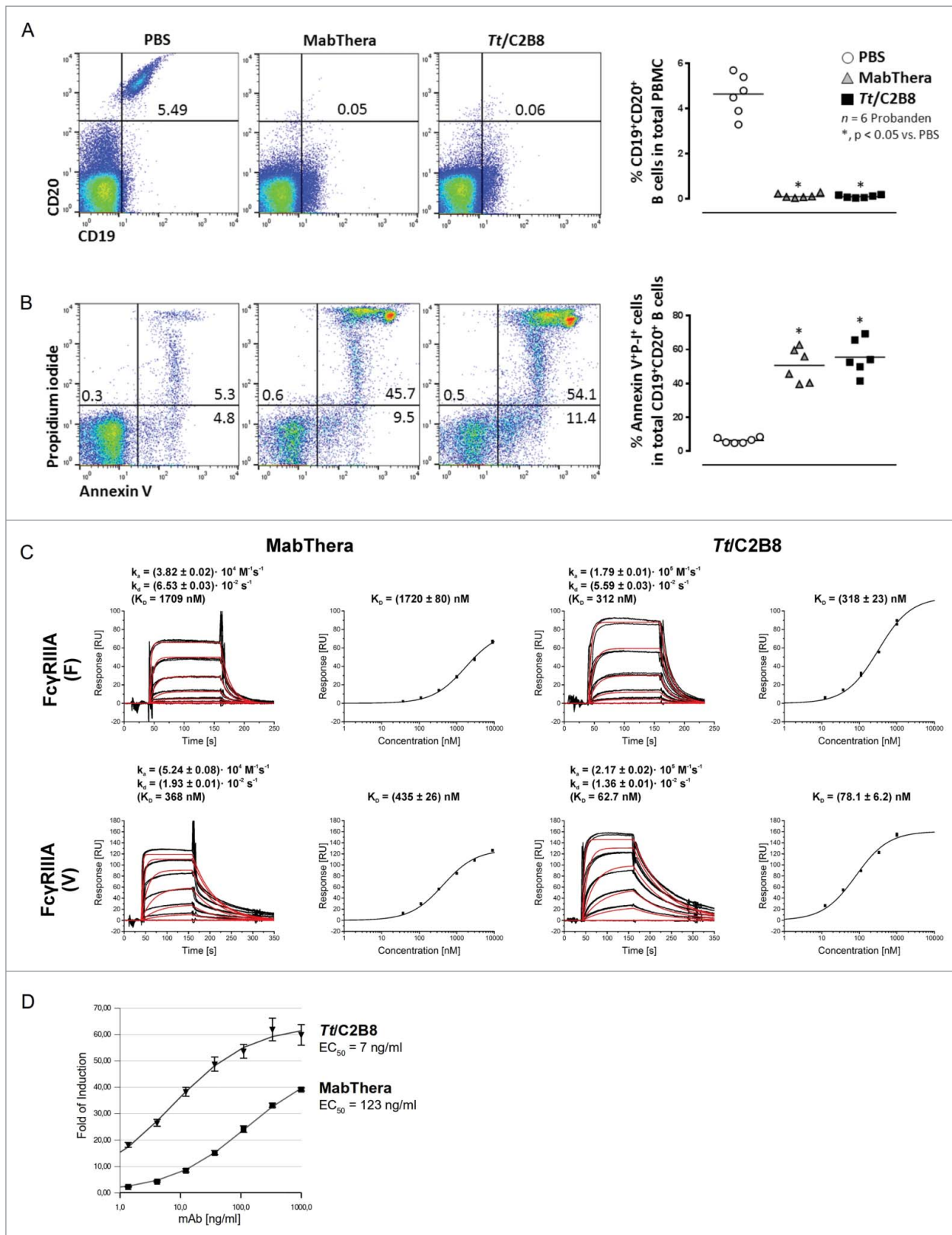


**Figure 3.** *In vitro* properties of anti-CD20 antibody expressed by *T. thermophila* and mammalian cells. (A) Both anti-CD20 antibodies bind to the CD20 epitope on human B cells in the same manner. Representative flow cytometry blots of freshly isolated PBMCs after incubation with MabThera<sup>®</sup> or Tt/C2B8. Control: PBMC incubated with PBS. (B) Induction of apoptosis in human PBMCs treated either with Tt/C2B8 or MabThera<sup>®</sup>. Representative flow cytometry blots of CD19/CD20 positive B cells gated for CD19 positive cells and stained with propidium iodide (P-I) and Annexin V. Apoptotic cells appear in upper right. (C) Interaction of immobilised human Fc $\gamma$ RIIIA F and V with anti-CD20 antibodies in a Biacore 3000 on a CM5 sensor chip (GE Healthcare). Serial dilutions (1:3, starting at 9  $\mu$ M) of MabThera<sup>®</sup> and Tt/C2B8 were injected in triplicates. Binding curves (colored graphs) were fitted according to the Langmuir 1:1 interaction model for the calculation of kinetic constants. Dissociation constants ( $K_D$ ) indicating the affinities of the receptor variants to the antibody samples were calculated from equilibrium responses. Bars indicate standard errors. (D) Induction of antibody-dependent cell-mediated cytotoxicity. Serial dilutions of fully glycosylated Tt/C2B8 (triangle) or MabThera<sup>®</sup> (square) were incubated with Raji-target cells and engineered Jurkat effector cells (ET-ratio 1 : 6). Luciferase activity was quantified using Bio-Glo<sup>TM</sup> reagent. Data were fitted using 4PLC curve fit and  $EC_{50}$  was calculated from the point of inflection. The y-axis error bars (SEM) result from  $n = 5$  separate replicates.

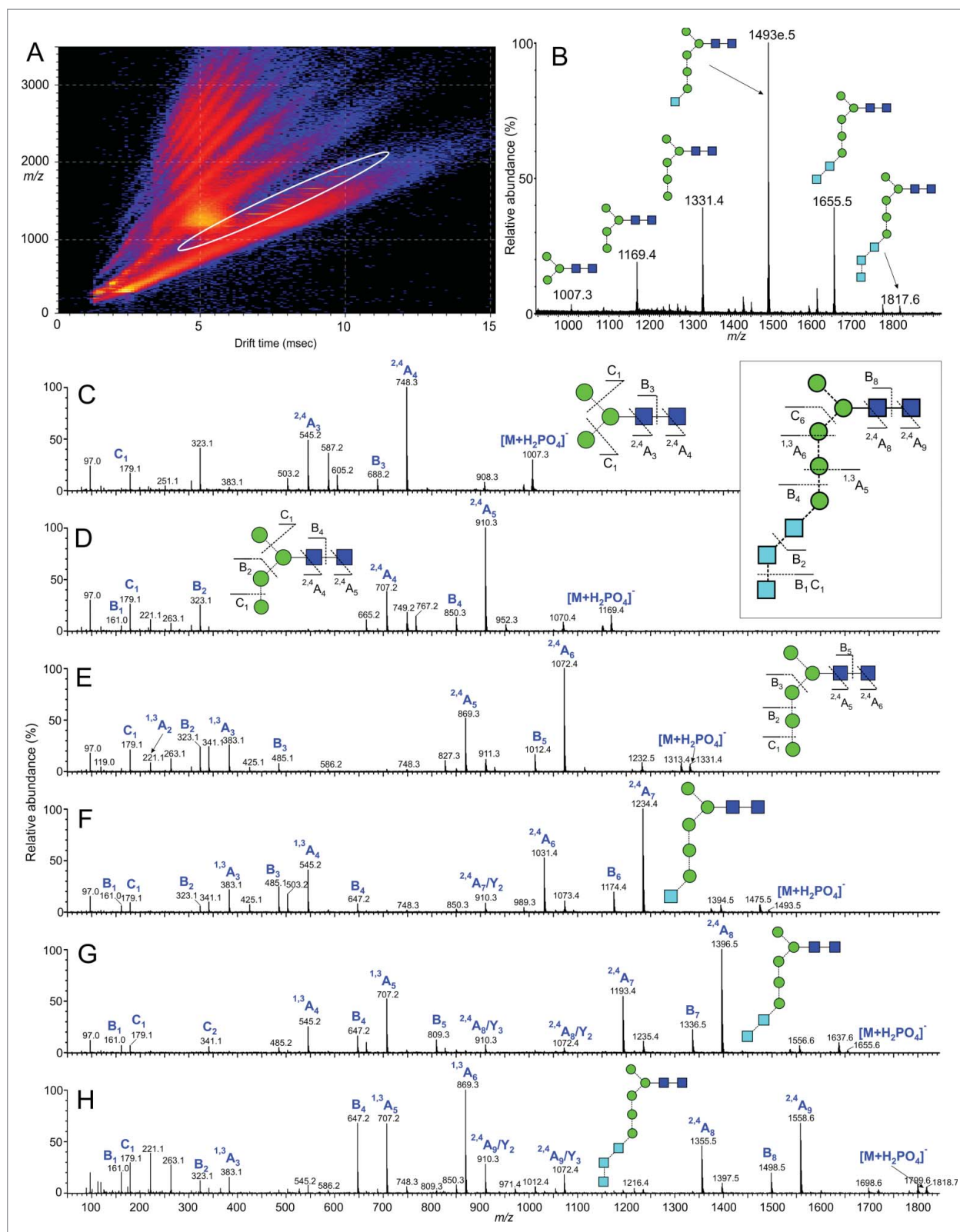


**Figure 4.** Ion mobility mass spectrometry analysis of Tt/C2B8. DriftScope image ( $m/z$  against drift time) of glycans released from Rituximab. The ions encircled with the white oval are from the singly charged N-glycans. (B) Mobility extracted singly charged ions from N-glycans released from rituximab (MabThera®), encircled region from panel A). (C-H) Collision-induced dissociation spectra from the transfer region of the Synapt G2Si instrument of the 6 N-glycans. The inset to panels C and D shows the numbering of the fragments for the  $\text{GlcNAc}_3\text{Man}_5\text{GlcNAc}_2$  glycan (from panel H). The numbering scheme follows that proposed by Domon and Costello.<sup>41</sup> Glycan symbols were assigned as depicted in the key in Fig. 2.

$\text{Glc}_{1-3}\text{Man}_5\text{GlcNAc}_2$ . The glycan identity was confirmed by collision-induced fragmentation of negative ( $[\text{M}+\text{H}_2\text{PO}_4]^-$ ) ions<sup>41-46</sup> as follows:

The fragmentation spectrum of  $\text{Man}_3\text{GlcNAc}_2$  (Fig. 4C) contained  $^{2,4}\text{A}_4$ ,  $\text{B}_3$  and  $^{2,4}\text{A}_3$  ions at  $m/z$  748.3, 688.3 and 545.2, respectively, confirming the structure of the  $\beta$ 1,4-linked

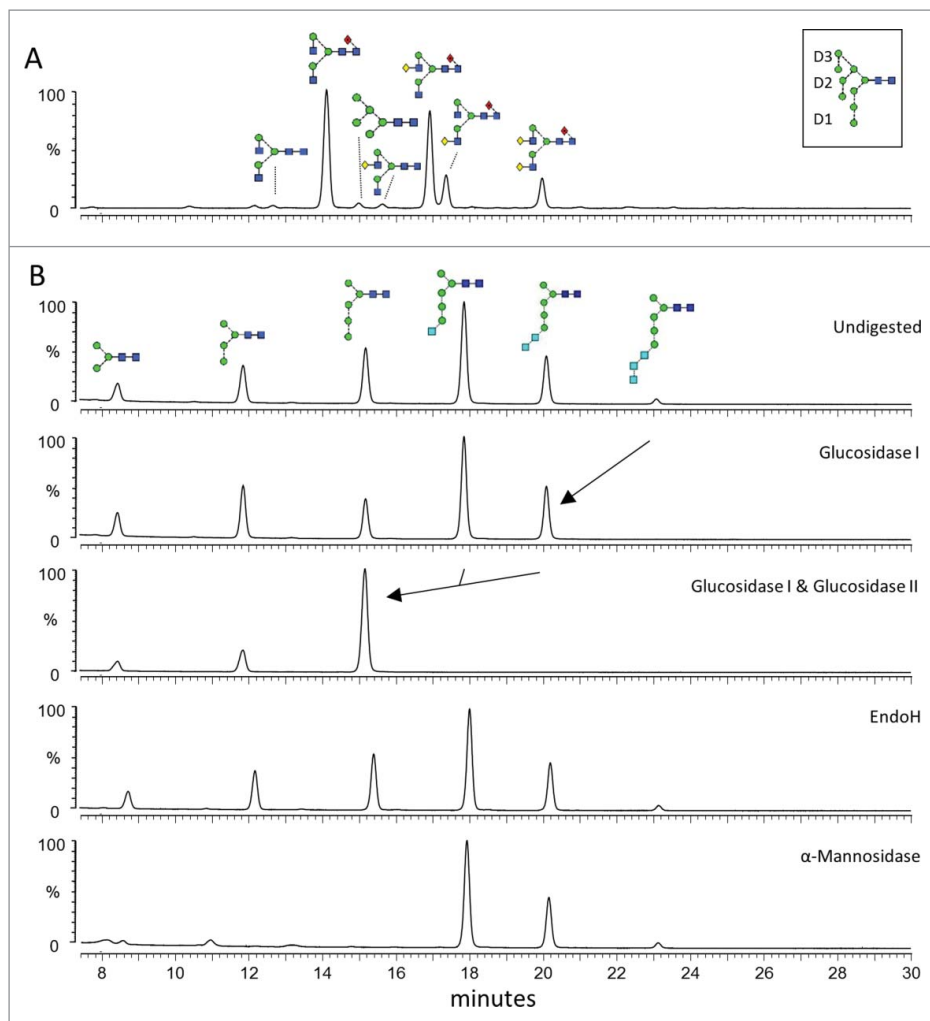


**Figure 5.** Fc N-glycan profiles of *Tt/C2B8* and Rituximab. (A) HILIC-UPLC spectra of fluorescently labeled N-linked glycans released from anti-CD20 antibody rituximab (MabThera<sup>®</sup>) produced in CHO cells. Assigned glycan structures are displayed as shown in Fig. 2. The inset in the top panel shows the labeling of D1, D2 and D3 arms on an exemplary  $\text{Man}_9\text{GlcNAc}_2$ . (B) HILIC-UPLC spectra of fluorescently labeled N-linked glycans released from *Tt/C2B8*. The undigested N-glycosylation profile is shown in the top panel. Structures were assigned using a panel of glycosidase digestions (glucosidase I, combined glucosidase I and II, Endoglycosidase H from *Streptomyces picatus* and  $\alpha(1-2,3,6)$ -mannosidase from Jack bean). Structural assignments were confirmed by ion-mobility ESI-MS/MS.

D-N-acetylchitobiose core in the absence of any substituents. The spectrum was identical to that of an authentic sample of  $\text{Man}_3\text{GlcNAc}_2$  obtained from chicken ovalbumin.<sup>44</sup> Ions corresponding to  $^{2,4}\text{A}_4$ ,  $\text{B}_3$  and  $^{2,4}\text{A}_3$  cleavages at masses consistent with their higher molecular weights (e.g.,  $m/z$  910.3, 850.3 and 707.2 in the spectrum shown in Fig. 4D) were present in the spectra of the other 5 glycans, again indicating no core-substitution. The spectra of oligomannose-type glycans substituted in the 6-antenna (6-arm) contain a prominent series of ions corresponding to  $^{1,4}\text{A}_2$ ,  $^{1,3}\text{A}_2$ , D-18 and D cleavages, where D-ions represent loss of the chitobiose core and the 3-antenna. No such ions were present in the spectra of the  $\text{Hex}_{4-8}\text{GlcNAc}_2$  glycans, showing that all additional hexoses were located in the 3-antenna. The spectrum of the glycan  $\text{Hex}_8\text{HexNAc}_2$  (Fig. 4H) contained abundant ions at  $m/z$  869.3, 809, 707.2, and 647.2. This pattern of ions, corresponding to  $^{1,3}\text{A}_6$ ,  $\text{B}_5$ ,  $^{1,3}\text{A}_5$  and  $\text{B}_4$  cleavages of the 3-antenna, combined with the results of glucosidase digestion, confirms the  $\text{Glc}_3\text{Man}_5\text{GlcNAc}_2$  structure for this glycan. Furthermore, this series of ions is prominent in the corresponding spectrum of  $\text{Glc}_3\text{Man}_7\text{GlcNAc}_2$  obtained from recombinant glycoproteins, such as

CD152 expressed in CHO cells in the presence of the glucosidase inhibitor NB-DNJ, further confirming the structure of the 3-antenna.<sup>44</sup> The spectrum of  $\text{Glc}_2\text{Man}_5\text{GlcNAc}_2$  (Fig. 4G) contains the same series of ions but with  $m/z$  values 162 mass units lower ( $m/z$  707, 647, 545, 485), reflecting the absence of the terminal glucose residue. Likewise, the shifts in  $m/z$  values of these ions in the spectra of  $\text{Glc}_1\text{Man}_5\text{GlcNAc}_2$  (Fig. 4F) and  $\text{Man}_5\text{GlcNAc}_2$  (Fig. 4E) reflect the absence of  $\text{Glc}_2$  and  $\text{Glc}_3$  units in these glycans, respectively, and confirm the structures shown in Fig. 5.

We performed HILIC-UPLC analysis of fluorescently labeled and released glycans from MabThera<sup>®</sup> and *Tt/C2B8* (Fig. 5). The commercially available MabThera<sup>®</sup> displays a glycosylation profile dominated by biantennary, fucosylated glycans. Glycan structures, as assigned in Fig. 5A, were confirmed by fragmentation through IM ESI-MS (data not shown). The profile of *T. thermophila* produced mAb (Fig. 5B) was confirmed by a panel of exo- and endoglycosidase digests. In particular, the presence of terminal glucose was verified by digestion with  $\alpha$ -glucosidases I and II. The most abundant structure is  $\text{Glc}_1\text{Man}_5\text{GlcNAc}_2$ . The

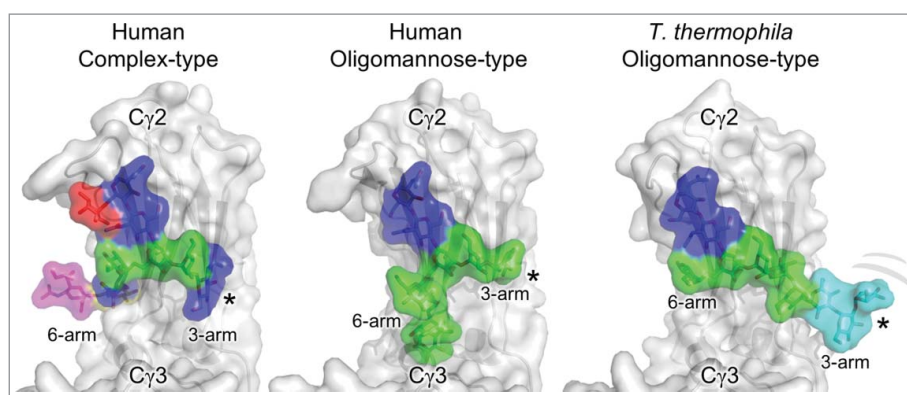


**Figure 6.** Glycoforms of the IgG Fc. Human and *T. thermophila* glycoforms of the IgG Fc C $\gamma$ 2 domain with the protein depicted in gray and the glycan residues shown as colored sticks with surface representation (red, fucose; blue, GlcNAc; green, mannose; cyan, glucose; magenta, sialic acid). The human complex-type glycoforms correspond to a region of the crystal structure of a hypersialylated Fc (PDB ID: 4BYH).<sup>76</sup> The human oligomannose glycoform shows the crystal structure of a Man<sub>9</sub>GlcNAc<sub>2</sub> in which discernible electron density was observed (PDB ID: 2WAH).<sup>67</sup> The *T. thermophila* oligomannose-type glycoform is a model of the Glc<sub>3</sub>Man<sub>9</sub>GlcNAc<sub>2</sub> isomer generated by the superimposition of the NMR structure of a glucosylated oligomannose glycan and the crystal structure of the Man<sub>3</sub>GlcNAc<sub>2</sub> glycoform (PDB ID: 1H3U).<sup>66,77</sup> The terminal residues of the 3-arm are disordered in the 2 crystal structures and we predict that the 3-arm in the *T. thermophila* oligomannose-type glycoforms is similarly conformationally flexible (\*).

insensitivity of the glycans to EndoH digestions (Fig. 5B) confirms that the isomers displayed by the ciliate oligomannose-type glycans lack the classical 6-arm branches of human glycans. Indeed, Endo H only requires a single mannosyl residue on the 6-arm on the trimannosyl core in order for cleavage to occur, which is consistent with our ion mobility fragmentation data (Fig. 4).<sup>47</sup> Additionally, our glycan assignments are entirely in accordance with the annotated genes for glycan biosynthesis in the *T. thermophila* genome.<sup>48</sup>

## Discussion

The clinical efficacy of mAbs has been firmly established, and consequently there is substantial research and development activity to further broaden clinical indications and to enhance patient outcomes. By 2014, forty-seven mAbs products had been approved for clinical use in the US or Europe. Only three of these were produced in a non-mammalian expression system (*E. coli*).<sup>49</sup> In order to meet the demand for therapeutic antibodies, nearly 10 t were produced in 2013 compared to about 8.6 t of all other recombinant products.<sup>30</sup> Generation of mammalian cell lines with high productivity, stable long term expression and good product quality is laborious and time consuming, the production costs are relatively high and the handling is very demanding. Mammalian cells, for instance, are susceptible to impurities and contaminations and sensitive toward liquid-associated shear stress because they are about 10- to 50-fold larger and more vulnerable than microbial cells.<sup>50</sup>

Despite their disadvantages, mammalian cell lines have become the dominant production system for mAb products. This is mainly because of their ability to perform required protein folding, assembly and posttranslational modifications, yielding in proteins that are biochemically similar to human ones. Furthermore, as a result of improvements in mammalian cell culture technology, productivity increased from 10 pg antibody per cell per day in 1986 to ~5 g/L in 2004, and yields can be ~12 g/L in CHO cells today.<sup>51</sup> However, the number of antibody products and the total volume needed by patients will

likely increase in the future. As a result, there is still a high demand for improvement of several aspects of mammalian cell culture (lowering the long timeline required for generation of a cell line or the product quality and stability) to lower the costs of antibody production, as well as development of new production systems and technologies.<sup>52</sup>

Here, we introduce a new promising technology for the production of recombinant therapeutic antibodies based on the unicellular eukaryotic protozoan *T. thermophila*. We demonstrate that the expression and secretion of a fully assembled monoclonal anti-CD20 antibody that exhibits the same antigenic properties, but increased affinity for the Fc $\gamma$ RIIIA and higher ADCC activity, compared to the commercially available, CHO cell-produced anti-CD20 antibody (MabThera<sup>®</sup>, Roche).

We observed a small proportion of potentially C-terminal lysine-clipped HCs in the native mass spectrometry analysis of the deglycosylated *Tt*/C2B8 antibody, which is a commonly observed variant of biopharmaceutical mAbs.<sup>53</sup> Antibodies of the IgG class derived from human B cells exhibits Fc domain glycosylation comprising the conserved pentasaccharide core (Man<sub>3</sub>GlcNAc<sub>2</sub>) modified by  $\beta$ 1,2-GlcNAc residues on each arm with the variable addition of further monosaccharides like bisecting GlcNAc residues, galactose, sialic acid and fucose.<sup>54</sup> The glycosylation pattern can not only vary between different antibodies, but also between both C $\gamma$ 2 domains of the same antibody.<sup>55</sup> Furthermore, Rustandi *et al.*<sup>56</sup> demonstrated that most therapeutic antibodies contain small but detectable amounts of aglycosylated HCs. These differences in glycosylation can lead to hemiglycosylation of the Fc region of the antibody.

Hemiglycosylated antibodies appear when an aglycosylated HC pairs with a glycosylated HC to form an IgG. *T. thermophila* secreted glycosylation variants of the anti-CD20 HC, and we could demonstrate a 5-fold increased binding affinity to the Fc $\gamma$ RIIIA, even though it has been shown by Ha *et al.*<sup>37</sup> that hemiglycosylated antibodies show significantly decreased binding affinities toward all Fc receptors when compared to fully glycosylated antibodies. We therefore hypothesized that the antibody-dependent cytotoxicity of a fully glycosylated *T. thermophila* produced C2B8 might be much higher than



MabThera<sup>®</sup>, which is produced in CHO cells. For the measurement of the ADCC effector function we applied the fully glycosylated fraction of the *Tt/C2B8* and could demonstrate an ~17-fold increase in antibody-dependent cytotoxicity compared MabThera<sup>®</sup>. ADCC assays are a good model of *in vivo* activity, but we note that their performance does not fully capture all physiological effects, such as the role of immune complex formation and the inhibitory role of competing endogenous IgG.<sup>57-59</sup>

These caveats aside, one reason for this increased performance is likely to be found in the fucose-free glycosylation pattern of *T. thermophila*. The major N-linked glycans found on human IgGs or IgGs produced by mammalian cells contain a fucose residue in an  $\alpha$ 1,6 position linked to the core GlcNAc residue (core fucose).<sup>54</sup> It has been shown that the removal of the core fucose, for instance by  $\alpha$ 1,6-fucosyltransferase gene (*FUT8*) knockout or by overexpression of heterologous  $\beta$ 1,4-*N*-acetylglucosaminyltransferase III (GnTIII), increases the affinity to Fc $\gamma$ RIIIA and, therefore, increases the ADCC activity of the IgG antibody.<sup>25</sup> The lack of fucose in the *T. thermophila* glycosylation pattern does seem to enhance the ADCC effector function of the anti-CD20 antibody. However, the lack of fucose at the core GlcNAc is likely not solely responsible for the modulated effector function. Another aspect to consider is the conserved biantennary core structure of the N-linked glycan attached to Asn<sup>297</sup> in the Fc domain containing up to 5 mannose residues and up to 3 glucose residues. SPR binding studies with homogeneous IgG-Fc glycoforms with defined core N-linked glycan transferred to the GlcNAc moiety by the transglycosylation activity of an *Arthrobacter* endoglycosidase (EndoA) showed that the presence of a bisecting GlcNAc or even a bisecting mannose residue could significantly enhance the binding of the Fc to Fc $\gamma$ RIIIA.<sup>22</sup> Additionally, it was shown that the  $\alpha$ -linked mannose residues in a Man<sub>3</sub>GlcNAc<sub>2</sub> core were essential to maintain the high affinity to the Fc $\gamma$ RIIIA.<sup>22</sup>

The observance of up to 3 terminal glucose residues on *Tt/C2B8* is in accordance with a report by Taniguchi *et al.*, who characterized 2 lysosomal enzymes secreted by a *T. pyriformis* strain.<sup>60</sup> They postulated an unusual dolichol pyrophosphate (Dol-PP) precursor (Glc<sub>3</sub>Man<sub>5</sub>GlcNAc<sub>2</sub>-DolPP instead of the Glc<sub>3</sub>Man<sub>9</sub>GlcNAc<sub>2</sub>-DolPP structure of yeast or mammalian cells). The terminal glucose residues are thought to be removed by  $\alpha$ -glucosidases I and II. There is a mammalian and yeast  $\alpha$ -glucosidase I homologous enzyme annotated (TTHERM\_00636930, mannosyl oligosaccharide glucosidase), which is possibly located in the endoplasmic membrane of *T. thermophila* and potentially able to remove  $\alpha$ 1,2-glucose residues.<sup>60</sup>

Taniguchi *et al.* analyzed a lysosomal  $\alpha$ -glucosidase II with an  $\alpha$ 1,3-linked glucose residue substrate specificity that is secreted by *T. thermophila*.<sup>60</sup> After removal of the terminal glucose residues of the N-linked glycans in yeast and mammalian cells, the resulting Man<sub>9</sub>GlcNAc<sub>2</sub> structure is further processed in the Golgi apparatus to generate hybrid or complex type glycans, starting with removal of  $\alpha$ 1,2-linked mannoses to generate a Man<sub>5</sub>GlcNAc<sub>2</sub> oligosaccharide precursor. Ciliates lack classical Golgi-associated enzymes to produce complex or hybrid-type glycan structures that are found in, for example, mammalian cells.<sup>61</sup> Additional processing could take place in the compartment of the secretory pathway or in the extracellular media, and could include trimming of up to 3 mannose residues ( $\alpha$ 1,2- and  $\alpha$ 1,3-linked). The necessary enzymes

have not yet been identified in *T. thermophila*, although there have been reports of  $\alpha$ -mannosidases of unknown specificity that are secreted alongside other lysosomal enzymes.<sup>62,63</sup>

Because the content and the composition of the lysosomal enzymes secreted by *T. thermophila* are strongly media-dependent,<sup>62,63</sup> the portfolio of the different N-linked glycans in *T. thermophila* might be influenced by the prevailing cultivation conditions. It remains to be determined if the observed range of N-glycan structures is the result of incomplete processing during intracellular transport, whether it is dependent on the resident time in the extracellular medium, or if it is the result of a normal variation.

Variations in the percentage of glycosylation level of mAb HC were observed in cultures of different *T. thermophila* clones (data not shown). Based on the publications of Hossler *et al.*<sup>63</sup> and Rouiller *et al.*,<sup>64</sup> we are currently testing different media formulations, and, in combination with an advanced clone screening procedure, we will be able to select high producer clones with the highest percentage of glycosylated mAb HC.

Regardless of the biosynthetic origin of the glycan structures and heterogeneity, the observed N-glycan structures, including terminal glucose residues, do not negatively influence the binding properties to the Fc $\gamma$ RIII or the ADCC effector function. We can rationalize these properties by the analysis of known crystal structures of IgG1 Fc glycoforms. Typical mammalian oligomannose structures contain a branched 6-arm that prevents the Man<sub>3</sub> moiety from fully relaxing against the protein surface, as is observed in Fc domains containing complex-type glycosylation.<sup>65,19</sup> In *T. thermophila*, the absence of such 6-arm branching would generate a 6-arm conformation resembling that described by Krapp *et al.* for the Man<sub>3</sub>GlcNAc<sub>2</sub> glycan.<sup>66</sup> Similarly, the extended mannosylated 3-arm would structurally resemble that reported by Crispin *et al.* for the Man<sub>9</sub>GlcNAc<sub>2</sub> glycoform.<sup>67</sup> In this way, the whole 3-arm projects into the interstitial space. The absence of resolvable density for the D1 mannose in the crystal structure of the Man<sub>9</sub>GlcNAc<sub>2</sub> glycoform would lead us to predict that both the D1 mannose and glucose cap in the *T. thermophila* glycoforms are very highly solvated and flexible (Fig. 6). In summary, while the *T. thermophila* glycans presented here diverge from those of human oligomannose-type glycans, their branches appear identical to sections of human glycans. The presence of terminal mannose residues on IgG Fc glycans has been shown to suppress serum half-life.<sup>68</sup> However, the influence of the capping glucose within the Fc on pharmacokinetics and immunogenicity has yet to be determined.

Taken together, the scalability of antibody production in *T. thermophila* and associated unique human-like glycosylation presents new opportunities for the manufacture of therapeutic antibodies with tuned pharmacokinetic properties and effector functions.

## Material and methods

### Constructs

We used a synthetic gene for the LC and the HC of the mAb that was codon-optimised according to the *T. thermophila* codon bias that is used for mainly high expressed genes. The sequences of the anti-CD20 was based on US patent 6,682,734.

Synthetic genes were cloned into intermediate plasmids and were thereby successfully assembled with the *PGP1 T. thermophila* signal sequence<sup>69</sup> (18AA, polyglycylated protein 1, accession no. DQ418790), the promoter and the terminator. The final expression cassette for the HC of the anti-CD20 antibody carried a 1 kb fragment of the *MTT1* promoter-active region, the *BTU2* terminator sequence of the *neo2* cassette and was cloned into a pAX\_vector derivative, which is based on the pAX-plasmid constructed by Weide *et al.*<sup>8</sup> The final expression cassette for the LC of the anti-CD20 antibody carried a 1.2 kb fragment of the *MTT5* promoter-active region, the *BTU2* terminator sequence of the *neo2* cassette and was cloned into a pKOIX-based integrative expression vector by Cre/Lox recombination. In the utilized pKOIX-vector-variant, the *neo* selection cassette was replaced by a *bsd* selection cassette (pKOIX\_B\_LC).<sup>8</sup> The employed plasmids were cloned by standard methods (details on intermediate plasmids and primers are available from the authors).

### Strains, cultivation and transformation of *T. thermophila*

*T. thermophila* inbred strains B1868/4 and B1868/7 were used as transformation hosts. Conjugating cells were transformed with the integrative expression vector (pKOIX\_B\_LC) *via* biolistic bombardment using standard protocols.<sup>11,70</sup> Afterwards, individual transformants were further cultivated at 30°C without agitation in 1.5 mL SPP medium (1% proteose peptone no 3, 0.5% yeast extract, 0.1% ferrous sulfate chelate solution, 0.2% glucose) supplemented with 10  $\mu$ /mL thymidine and increasing concentrations of the antibiotic blasticidin (from 50  $\mu$ g/mL to 500  $\mu$ g/mL) for several passages to support the allelic assortment process. Thymidine auxotrophic single cell clones were cotransformed with the episomal expression vector (pAX\_hNeoR\_HC) *via* biolistic bombardment using standard protocols. Transformants were further cultivated at 30°C without agitation in 1.5 mL SPP medium supplemented with 10  $\mu$ /mL thymidine and 300  $\mu$ g/mL paromomycin. Small-scale cultivation was performed in 1.5 mL SPP-medium at 30°C at 80 rpm in a Multitron AJ incubation shaker (Infors AG).

### SDS-PAGE, western blot analysis and silver staining

Protein expression and secretion into the supernatant was verified by SDS-PAGE on 4–20% bis-tris gels (Anamed Elektrophorese GmbH).<sup>71</sup> Gels were either blotted onto nitrocellulose membranes or stained according to Pierce<sup>®</sup> Silver Stain Kit (Thermo Scientific). Blotted nitrocellulose membranes were blocked in phosphate-buffered saline (PBS) containing 0.05% Tween 20 and 5% skim milk (PBS-TM). Expression of recombinant anti-CD20 antibody in transformed ciliates was detected by a polyclonal horseradish peroxidase (HRP)-conjugated goat-anti-human IgG antibody (H<sup>+</sup>L) (A8792, Sigma). The blots were developed by using chemiluminescence. Western blots were visualized using a Fusion imaging system and software (Peqlab).

### ELISA analysis of anti-CD20 antibody secretion level

Aliquots of supernatant were assayed in a quantitative sandwich ELISA using MabThera<sup>®</sup> (Roche) for creation of standard curves. For the assay, Nunc MaxiSorp<sup>®</sup> 96-well plates were coated with recombinant protein A (Thermo Scientific) at a concentration of 5  $\mu$ g/mL and the bound antibody was detected by HRP-conjugated goat F(ab')<sub>2</sub> anti-mouse IgG (Fab')<sub>2</sub> (ab98659, Abcam). Peroxidase reaction was started using Ultra TMB ELISA reagent (Fermentas) and measured at 450 nm using spectral photometer (Bio-Tek Instruments).

### Lab scale fermentation

Fedbatch fermentations of *T. thermophila* were conducted in a 6x 0.5L multifermenter (Sixforse, Infors AG). The fermenter was inoculated with 40  $\times$  10<sup>3</sup> cells/mL and cells were grown in a modified SPP medium (2.5% proteose peptone no 3, 1% peptone acid hydrolysate from vegetable, 0.5% yeast extract, 0.1% ferrous sulfate chelate solution, 0.2% glucose), supplemented with 260  $\mu$ g/mL paromomycin and 10  $\mu$ g/mL thymidine. The temperature was maintained at 30°C and pO<sub>2</sub> was controlled at 20% of the air saturation level by stirrer speed (500–1000 rpm) and air flow (0.1–0.5 L/min). The pH value was regulated to pH 7.0 during the fermentation process.

Anti-CD20 antibody expression was induced by the addition of 10  $\mu$ g/mL cadmium chloride to the culture medium at a cell density of 1.5–1.8  $\times$  10<sup>6</sup> cells/mL. The culture supernatant was harvested 24 h after induction of protein by stepwise centrifugation (15 min 1,500 g at 12°C and 30 min 14,000 g at 4°C). Supernatants were stored immediately at –80°C.

### PNGase F treatment

Samples consisting of 18  $\mu$ L supernatant and 2  $\mu$ L 10 $\times$  denaturation buffer were boiled for 10 min. After that 3  $\mu$ L of 10 $\times$  G7 deglycosylation buffer, 3  $\mu$ L of 10% NP40 and 2  $\mu$ L of PNGase F (New England Biolabs) were added and adjusted to 30  $\mu$ L. Aliquots of these reactions were analyzed by SDS-PAGE and western blot and CE-SDS.

### Cation-exchange HPLC

After Protein A affinity purification of the anti-CD20 antibody, the differently glycosylated variants were separated as described previously<sup>72</sup> on a Hitachi LaChrom Elite<sup>®</sup> HPLC System using a ProPac WCX-10 (4  $\times$  250 mm) column (Thermo Fischer) and a salt gradient elution at pH 4.0 (mobile phase A: 10 mM sodium acetate, pH 4.0; mobile phase B: 10 mM sodium acetate pH 4.0, 1.0 M NaCl). A constant flow rate of 1 mL/min was maintained and the NaCl gradient was increased 1% per minute, which is equivalent to 10 mM NaCl increase per minute.

### CE-SDS gel using Bioanalyzer 2100

CE-SDS of the protein probes was performed in Bioanalyzer 2100 (Agilent Technologies) on a High Sensitivity Protein Chip to determine the ratio of glycosylated and aglycosylated HC molecules in antibody samples. Sample preparation was

performed using Agilent High Sensitivity Protein 250 Kit (Agilent Technologies) according to the manufacturer's instructions. To detect the proteins, a labeling reaction was performed. Quantification and size analysis were based on a protein standard as a reference in every measurement using Bioanalyzer 2100 system and software.

### **Purification of anti-CD20 antibody expressed by *T. thermophila***

Cell-free supernatants harvested from fermentation processes were applied to a Protein A agarose column (mABSelectSuRe, GE Healthcare) equilibrated with 10 mM phosphate buffer containing 140 mM sodium chloride (pH 7.2). Antibodies were eluted after washing the column (5 CV) with equilibration buffer using 100 mM glycine - HCl (pH 2.9) and neutralized by 1 M Tris - HCl (pH 9.0). In antibody-containing fractions, a buffer exchange into stabilizing buffer (9 mg/L NaCl, 7.35 mg/L sodium citrate dihydrate, 0.7 mg/L polysorbate 80, pH 6.8) was performed using Vivaspin 20 columns (Sartorius).

### **Native mass spectrometry**

Native mass spectrometry measurements were performed on a hybrid quadrupole-Orbitrap instrument modified for detection of high mass ions. Samples (20  $\mu$ M) were buffer exchanged into 200 mM ammonium acetate using Bio-spin 6 (Bio-Rad) centrifuge columns immediately prior to analysis. Ions were generated by static nanoelectrospray using gold-coated capillaries prepared in-house. Data were obtained with a wide acquisition window (1,000–15,000  $m/z$ ) and desolvation was achieved with HCD voltage applied (200 V). Additional instrument settings were as follows: capillary voltage = 1.2 kV; source temperature = 60°C; max injection time = 50; S-lens RF = 100; C-trap entrance lens = 5.8. Spectra were obtained with 10 microscans, averaged over 50 scans. Data was processed using XCalibur 2.1 software (Thermo Scientific) and masses were assigned using in-house software.

### **Fc $\gamma$ R binding affinities of mAbs**

Binding affinities of Fc $\gamma$ R variants to anti-CD20 antibodies were determined by SPR using a Biacore 3000 (GE Healthcare). According to the manufacturer's protocol, anti-histidine antibody (HIS capture Kit, GE Healthcare) was covalently bound to the carboxymethylated dextran matrix of a CM5 sensor chip using the His Capture Kit (GE Healthcare). Afterwards, recombinant histidine-tagged human ectodomains of Fc $\gamma$ R1IIIA variants (Sino Biological) were immobilized onto the surface using a previously published protocol.<sup>73</sup>

Antibody samples were diluted serially (1:3) in running buffer HBS-EP (GE Healthcare) starting at 9  $\mu$ M MabThera<sup>®</sup> or 1  $\mu$ M Tt/C2B8 and injected at a flow rate of 30  $\mu$ l/min into the flow cells. Associations and dissociations were monitored for 120 s, respectively. The measurements were performed in triplicates and in random order. Evaluation of the data was done using BIAevaluation software (GE Healthcare). The equilibrium fit, based on the steady state responses, was used to give the  $K_D$ -value (1:1 binding model). Moreover, binding

curves were fitted to a monoexponential 1:1 binding model to obtain association and dissociation rate constants, as well as the  $K_D$ -value. The response of the reference flow cell without captured ligand but with anti-His antibody and blank injections of running buffer were subtracted from each binding curve prior to analysis.

### **ADCC Reporter Bioassay**

The ADCC Reporter Bioassay (Promega) was used to evaluate the Fc-mediated effector function of the anti-CD20 antibodies. According to the manufacturer's instructions, Raji target cells and Jurkat/NFAT-luc effector cells were thawed just before the assay. The cells were suspended in Roswell Park Memorial Institute (RPMI) medium (effector/target ratio 6:1) and cocultured in the presence of serially diluted anti-CD20 antibody samples. After incubation for 6 h at 37°C, luciferase activity was quantified using BioGlo<sup>™</sup> reagent (Promega) and fluorescence reader (Bio-Tek Instruments). Data were fitted by 4PLC curve fit and EC<sub>50</sub> was calculated from the point of inflection. Measurements were done in triplicates and 5 independent experiments were performed.

### **Enzymatic in-gel release of N-linked glycans**

Coomassie blue-stained antibody bands (40  $\mu$ g) were excised from SDS gels and washed alternately with acetonitrile and water. The gel slices were rehydrated in 20 mM sodium bicarbonate buffer (pH 7.0). N-linked glycans were released by the addition of 1  $\mu$ L PNGase F (New England Biolabs), incubated for 16 h at 37°C and extensively washed out of the gel matrix with water. Released glycans were then dried using a SpeedVac concentrator (Eppendorf) and either fluorescently labeled with 2-aminobenzoic acid (2-AA) or analyzed by ion mobility ESI-MS/MS.

### **Fluorescent labeling of N-linked glycans**

Enzymatically released glycans were labeled with 2-AA as previously described.<sup>74</sup> Briefly, glycans were resuspended in 30  $\mu$ L water followed by the addition of 80  $\mu$ L labeling reaction mix, composed of 30 mg/mL 2-AA and 45 mg/mL sodium cyanoborohydride dissolved in sodium acetate trihydrate (4% w/v) and boric acid (2% w/v) in methanol. After incubation at 80°C for 60 min, excess fluorescent label was removed employing Speed Amide-2 cartridges, followed by HILIC-UPLC analysis.

### **HILIC-UPLC analysis of N-linked glycans**

Glycans labeled with 2-AA were chromatographically separated by HILIC-UPLC using a 2.1 mm  $\times$  10 mm Acquity BEH Amide Column (1.7  $\mu$ m particle size, Waters) in a Waters Acquity UPLC instrument. The following gradient was applied: time = 0 min ( $t = 0$ ): 22% A, 78% B (0.5 mL/min);  $t = 38.5$ : 44.1% A, 55.9% B (0.5 mL/min);  $t = 39.5$ : 100% A, 0% B (0.25 mL/min);  $t = 44.5$ : 100% A, 0% B;  $t = 46.5$ : 22% A, 78% B (0.5 mL/min), where solvent A was 50 mM ammonium formate, pH 4.4 and solvent B was acetonitrile. Fluorescence

measuring occurred at an excitation wavelength of 428 nm. Empower 3 software was used for data processing.

### Glycosidase digestions of N-linked glycans

For purposes of structure determination, 2-AA labeled glycans were resuspended in water and digested using a panel of endo- and exo-glycosidases. The enzymes used were Endoglycosidase H from *Streptomyces picatus* (P0702, New England Biolabs),  $\alpha$ -L-fucosidase from bovine kidney (F5884, Sigma),  $\beta$ 1,4-galactosidase from *Streptococcus pneumoniae* (E-BG07, QA Bio) and  $\alpha$ (1-2,3,6)-mannosidase from Jack bean (EAM01, QA Bio). Glucosidase I (N-terminal truncated enzyme) and II (full length) from *mus musculus* were kindly provided by Alessandro Caputo (Glycobiology Institute, University of Oxford). Digestion reactions were performed for 16 h at 37°C, according to manufacturer's instructions. Following digestion, glycans were cleaned using a polyvinylidene fluoride protein-binding membrane plate (MAIPS4510, Millipore).

### Ion mobility mass spectrometry analysis of released glycans

Aqueous solutions (1  $\mu$ L) of the samples were cleaned with a Nafion® 117 membrane. They were then reconstituted in methanol:water (1:1, v:v, 8  $\mu$ L) containing ammonium phosphate (0.05 M) and infused with Waters thin-wall nanospray capillaries into a Waters Synapt G2Si traveling wave ion mobility mass spectrometer (Waters, Manchester, UK) fitted with a nano-electrospray (ESI) ion source operated in negative ion mode. Instrumental conditions were: ESI capillary voltage, 1.0–1.2 kV; cone voltage, 150 V; ion source temperature, 80°C; T-wave velocity; 450 m/sec; T-wave peak height 40 V. Fragmentation by collision-induced dissociation (CID) was performed after mobility separation in the transfer cell with argon as the collision gas. The instrument was mass calibrated with caesium iodide. Data acquisition and processing were carried out using the Waters DriftScope (version 2.8) software and MassLynx™ (version 4.1). The scheme devised by Domon and Costello<sup>41</sup> was used to name the fragment ions.

### Disclosure of potential conflicts of interest

J.C., S.M., U.B. and M.W.W.H. are employees of Cilian AG. No other conflicts of interests were disclosed.

### Acknowledgments

We would like to thank Jan Rossdorf for excellent technical assistance, Maren Wieholt from Wessling GmbH for preparative separation of glycosylated variants and Madeline Möller for support with the SPR analysis. We thank Ingo Aldag and Karina Jawinski for valuable discussions, review of the manuscript and support for this work. This work has in part been funded through the program “KMU Innovativ 6” by the German Federal Ministry of Education and Research (0315856).

This work in the laboratory of M.C. was supported by a grant from Against Breast Cancer and an equipment grant to purchase the Synapt mass spectrometer from the International AIDS Vaccine Initiative Neutralizing Antibody Center and NAC CAVD grant. M.C. is the Against Breast Cancer Fellow in Cancer Therapeutics at Oriel College, Oxford.

A.J.B. is supported by the Chris Scanlan Memorial Scholarship at Corpus Christi College, Oxford.

The work of M.M.N. is supported by infrastructure of the cluster of Excellence RESOLV (EXC 1069) funded by the Deutsche Forschungsgemeinschaft.

### ORCID

Anna-Janina Behrens  <http://orcid.org/0000-0002-4270-6744>  
 Sonja Mader  <http://orcid.org/0000-0002-5393-1015>  
 David J. Harvey  <http://orcid.org/0000-0003-0544-771X>  
 Kai U. Cormann  <http://orcid.org/0000-0003-0772-6456>  
 Daniel Schinor  <http://orcid.org/0000-0003-2708-9853>  
 Marcus W.W. Hartmann  <http://orcid.org/0000-0002-4395-693X>

### References

- Collins K, Gorovsky M. *Tetrahymena thermophila*. Curr Biol 2005; 15: R317-8; PMID:15886083; <http://dx.doi.org/10.1016/j.cub.2005.04.039>
- Wheatley D, Rasmussen L, Tiedtke A. *Tetrahymena*: a model for growth, cell cycle and nutritional studies, with biotechnological potential. Bioessays 1994; 16:367-72; PMID:8024545; <http://dx.doi.org/10.1002/bies.950160512>
- Kiy TT. Mass cultivation of *Tetrahymena thermophila* yielding high cell densities and short generation times. Appl Microbiol Biotechnol 1992; 37:576-9; <http://dx.doi.org/10.1007/BF00240728>
- Clark T, Zhang X, Jayaram J, Appleton J, Bisharyan Y, Gagliardo L, Colussi P, Papoyan A, Cassidy-Hanley D. An Alternative Platform for Rapid Production of Effective Subunit Vaccines, *Tetrahymena thermophila* offers numerous advantages as an expression system, including rapid cell growth and high cell densities, eukaryotic protein folding, and active synthesis of membrane and secreted proteins. BioPharm Int 2010; 2:1-6.
- Stover N, Krieger C, Binkley G, Dong Q, Fisk D, Nash R, Sethuraman A, Weng S, Cherry J. *Tetrahymena* Genome Database (TGD): a new genomic resource for *Tetrahymena thermophila* research. Nucleic Acids Res 2006; 34:D500-3; PMID:16381920; <http://dx.doi.org/10.1093/nar/gkj054>
- Eisen JA, Coyne RS, Wu M, Wu D, Thiagarajan M, Wortman JR, Badger JH, Ren Q, Amedeo P, et al. Macronuclear genome sequence of the ciliate *Tetrahymena thermophila*, a model eukaryote. PLoS Biol 2006; 4:e286; PMID:16933976; <http://dx.doi.org/10.1371/journal.pbio.0040286>
- Xiong J, Lu X, Lu Y, Zeng H, Yuan D, Feng L, Chang Y, Bowen J, Gorovsky M, et al. *Tetrahymena* Gene Expression Database (TGED): a resource of microarray data and co-expression analyses for *Tetrahymena*. Sci China Life Sci 2011; 54: 65-67; PMID:21253873; <http://dx.doi.org/10.1007/s11427-010-4114-1>
- Weide T, Bockau U, Rave A, Herrmann L, Hartmann MWW. A recombinase system facilitates cloning of expression cassettes in the ciliate *Tetrahymena thermophila*. BMC Microbiol 2007; 7:12; PMID:17328820; <http://dx.doi.org/10.1186/1471-2180-7-12>
- Herrmann L, Bockau U, Tiedtke A, Hartmann MWW, Weide T. The bifunctional dihydrofolate reductase thymidylate synthase of *Tetrahymena thermophila* provides a tool for molecular and biotechnology applications. BMC Biotechnol 2006; 6:21; PMID:16549005; <http://dx.doi.org/10.1186/1472-6750-6-21>
- Gaertig J, Gorovsky MA. Efficient mass transformation of *Tetrahymena thermophila* by electroporation of conjugants. Proc Natl Acad Sci U S A 1992; 89:9196-200; PMID:1409625; <http://dx.doi.org/10.1073/pnas.89.19.9196>
- Cassidy-Hanley D, Bowen J, Lee JH, Cole E, VerPlank LA, Gaertig J, Gorovsky MA, Bruns PJ. Germline and somatic transformation of mating *Tetrahymena thermophila* by particle bombardment. Genetics 1997; 146:135-47; PMID:9136007
- Cowan GJM, Bockau U, Eleni-Muus J, Aldag I, Samuel K, Creasey A, Hartmann MWW, Cavanagh DR. A novel malaria vaccine candidate antigen expressed in *Tetrahymena thermophila*. PLoS One 2014; 9:e87198; PMID:24489871; <http://dx.doi.org/10.1371/journal.pone.0087198>
- Aldag I, Bockau U, Rossdorf J, Laarmann S, Raaben W, Herrmann L, Weide T, Hartmann MWW. Expression, secretion and surface display

- of a human alkaline phosphatase by the ciliate *Tetrahymena thermophila*. *BMC Biotechnol* 2011; 11:11; PMID:21281462; <http://dx.doi.org/10.1186/1472-6750-11-11>
14. Weide T, Herrmann L, Bockau U, Niebur N, Aldag I, Laroy W, Contreras R, Tiedtke A, Hartmann MWW. Secretion of functional human enzymes by *Tetrahymena thermophila*. *BMC Biotechnol* 2006; 6:19; PMID:16542419; <http://dx.doi.org/10.1186/1472-6750-6-19>
  15. Knaeblein J. *Modern Biopharmaceuticals: Recent Success Stories*. Knaeblein J. (Editor) Wiley-VCH Verlag GmbH & Co, KGaA; 2013.
  16. Ravetch JV. Fc receptors. *Curr Opin Immunol* 1997; 9:121-25; PMID:9039776; [http://dx.doi.org/10.1016/S0952-7915\(97\)80168-9](http://dx.doi.org/10.1016/S0952-7915(97)80168-9)
  17. Mimura Y, Church S, Ghirlando R, Ashton P, Dong S, Goodall M, Lum J, Jefferis R. The influence of glycosylation on the thermal stability and effector function expression of human IgG1-Fc: properties of a series of truncated glycoforms. *Mol Immunol* 2000; 37:697-706; PMID:11275255; [http://dx.doi.org/10.1016/S0161-5890\(00\)00105-X](http://dx.doi.org/10.1016/S0161-5890(00)00105-X)
  18. Rudd PM, Dwek RA. Glycosylation: heterogeneity and the 3D structure of proteins. *Crit Rev Biochem Mol Biol* 1997; 32:1-100; PMID:9063619; <http://dx.doi.org/10.3109/10409239709085144>
  19. Bowden TA, Baruah K, Coles CH, Harvey D, Yu X, Song B-D, Stuart DL, Aricescu A, Scanlan CN, et al. Chemical and structural analysis of an antibody folding intermediate trapped during glycan biosynthesis. *J Am Chem Soc* 2012; 134:17554-63; PMID:23025485; <http://dx.doi.org/10.1021/ja306068g>
  20. Dalziel M, Crispin M, Scanlan CN, Zitzmann N, Dwek RA. Emerging principles for the therapeutic exploitation of glycosylation. *Science* 2014; 343:1235681; PMID:24385630; <http://dx.doi.org/10.1126/science.1235681>
  21. Washburn N, Schwab I, Ortiz D, Bhatnagar N, Lansing JC, Medeiros A, Tyler S, Mekala D, Cochran E, et al. Controlled tetra-Fc sialylation of IVIg results in a drug candidate with consistent enhanced anti-inflammatory activity. *Proc Natl Acad Sci U S A* 2015; 112:E1297-306; PMID:25733881; <http://dx.doi.org/10.1073/pnas.1422481112>
  22. Zou G, Ochiai H, Huang W, Yang Q, Li C, Wang LX. Chemoenzymatic synthesis and Fc receptor binding of homogeneous glycoforms of antibody Fc domain. Presence of a bisecting sugar moiety enhances the affinity of Fc to FcIIIa receptor. *J Am Chem Soc* 2011; 133:18975-91; PMID:22004528; <http://dx.doi.org/10.1021/ja208390n>
  23. Yu M, Brown D, Reed C, Chung S, Lutman J, Stefanich E, Wong A, Stephan JP, Bayer R. Production, characterization, and pharmacokinetic properties of antibodies with N-linked mannose-5 glycans. *mAbs* 2012; 4:475-487; PMID:22699308; <http://dx.doi.org/10.4161/mabs.20737>
  24. Kanda Y, Yamada T, Mori K, Okazaki A, Inoue M, Kitajima-Miyama K, Kuni-Kamochi R, Nakano R, Yano K, et al. Comparison of biological activity among nonfucosylated therapeutic IgG1 antibodies with three different N-linked Fc oligosaccharides: the high-mannose, hybrid, and complex types. *Glycobiology* 2007; 17:104-18; PMID:17012310; <http://dx.doi.org/10.1093/glycob/cwl057>
  25. Beck A, Reichert JM. Marketing approval of mogamulizumab: a triumph for glyco-engineering. *mAbs* 2012; 4:419-425; PMID:22699226; <http://dx.doi.org/10.4161/mabs.20996>
  26. Cérutti M, Golay J. Lepidopteran cells, an alternative for the production of recombinant antibodies? *mAbs* 2012; 4:294-309; <http://dx.doi.org/10.4161/mabs.19942>
  27. Ha S, Wang Y, Rustandi R. Biochemical and biophysical characterization of humanized IgG1 produced in *Pichia pastoris*. *mAbs* 2011; 3:453-60; PMID:22048694; <http://dx.doi.org/10.4161/mabs.3.5.16891>
  28. Tada M, Tatematsu K, Ishii-Watabe A, Harazono A, Takakura D, Hashii N, Sezutsu H, Kawasaki N. Characterization of anti-CD20 monoclonal antibody produced by transgenic silkworms (*Bombyx mori*). *mAbs* 2015; 7:1-13; PMID:25484055; <http://dx.doi.org/10.4161/19420862.2015.988944>
  29. Platis D, Drossard J, Fischer R, Ma JK, Labrou NE. New downstream processing strategy for the purification of monoclonal antibodies from transgenic tobacco plants. *J Chromatogr A* 2008; 1211:80-89; PMID:18945431; <http://dx.doi.org/10.1016/j.chroma.2008.09.103>
  30. Yamane-Ohnuki N, Kinoshita S, Inoue-Urakubo M, Kusunoki M, Iida S, Nakano R, Wakitani M, Niwa R, Sakurada M, et al. Establishment of FUT8 knockout Chinese hamster ovary cells: an ideal host cell line for producing completely defucosylated antibodies with enhanced antibody-dependent cellular cytotoxicity. *Biotechnol Bioeng* 2004; 87:614-22; PMID:15352059; <http://dx.doi.org/10.1002/bit.20151>
  31. Umaña P, Jean-Mairet J, Moudry R, Amstutz H, Bailey JE. Engineered glycoforms of an antineuroblastoma IgG1 with optimized antibody-dependent cellular cytotoxic activity. *Nat Biotechnol* 1999; 17:176-80; PMID:10052355; <http://dx.doi.org/10.1038/6179>
  32. Zhang N, Liu L, Dumitru CD, Cummings NR, Cukan M, Jiang Y, Li Y, Li F, Mitchell T, et al. Glycoengineered *Pichia* produced anti-HER2 is comparable to trastuzumab in preclinical study. *mAbs* 2011; 3:289-98; PMID:21487242; <http://dx.doi.org/10.4161/mabs.3.3.15532>
  33. Wuitschick JD, Karrer KM. Analysis of genomic G + C content, codon usage, initiator codon context and translation termination sites in *Tetrahymena thermophila*. *J Eukaryot Microbiol* 1999; 46:239-47; PMID:10377985; <http://dx.doi.org/10.1111/j.1550-7408.1999.tb05120.x>
  34. Larsen LK, Andreassen PH, Dreisig H, Palm L, Nielsen H, Engberg J, Kristiansen K. Cloning and characterization of the gene encoding the highly expressed ribosomal protein l3 of the ciliated protozoan *Tetrahymena thermophila*. Evidence for differential codon usage in highly expressed genes. *Cell Biol Int* 1999; 23:551-60; PMID:10704239; <http://dx.doi.org/10.1006/cbir.1999.0419>
  35. Pedersen IM, Buhl AM, Klausen P, Geisler CH, Jurlander J. The chimeric anti-CD20 antibody rituximab induces apoptosis in B-cell chronic lymphocytic leukemia cells through a p38 mitogen activated protein-kinase-dependent mechanism. *Blood* 2002; 99:1314-19; PMID:11830481; <http://dx.doi.org/10.1182/blood.V99.4.1314>
  36. Smith MR. Rituximab (monoclonal anti-CD20 antibody): mechanisms of action and resistance. *Oncogene* 2003; 22:7359-68; PMID:14576843; <http://dx.doi.org/10.1038/sj.onc.1206939>
  37. Ha S, Ou Y, Vlasak J, Li Y, Wang S, Vo K, Du Y, Mach A, Fang Y, Zhang N. Isolation and characterization of IgG1 with asymmetrical Fc glycosylation. *Glycobiology* 2011; 21:1087-96; PMID:21470983; <http://dx.doi.org/10.1093/glycob/cwr047>
  38. Cartron G, Dacheux L, Salles G, Solal-Celigny P, Bardos P, Colombat P, Watier H. Therapeutic activity of humanized anti-CD20 monoclonal antibody and polymorphism in IgG Fc receptor FcγRIIIa gene. *Blood* 2002; 99:754-8; PMID:11806974; <http://dx.doi.org/10.1182/blood.V99.3.754>
  39. Natsume A, Niwa R, Satoh M. Improving effector functions of antibodies for cancer treatment: Enhancing ADCC and CDC. *Drug Des Devel Ther* 2009; 3:7-16; PMID:19920917
  40. Parekh BS, Berger E, Sibley S, Cahya S, Xiao L, LaCerte MA, Vaillancourt P, Wooden S, Gately D. Development and validation of an antibody-dependent cell-mediated cytotoxicity-reporter gene assay. *mAbs* 2012; 4:310-318; PMID:22531445; <http://dx.doi.org/10.4161/mabs.19873>
  41. Doman B, Costello CE. A systematic nomenclature for carbohydrate fragmentations in FAB-MS/MS spectra of glycoconjugates. *Glycoconj J* 1988; 5:397-409; <http://dx.doi.org/10.1007/BF01049915>
  42. Börnsen KO, Mohr MD, Widmer HM. Ion exchange and purification of carbohydrates on a Nafion(R) membrane as a new sample pretreatment for matrix-assisted laser desorption-ionization mass spectrometry. *Rapid Commun Mass Spectrom* 1995; 9:1031-34; <http://dx.doi.org/10.1002/rcm.1290091112>
  43. Giles K, Pringle SD, Worthington KR, Little D, Wildgoose JL, Bateman RH. Applications of a travelling wave-based radio-frequency-only stacked ring ion guide. *Rapid Commun Mass Spectrom* 2004; 18:2401-14; PMID:15386629; <http://dx.doi.org/10.1002/rcm.1641>
  44. Harvey D. Fragmentation of negative ions from carbohydrates: Part 2. Fragmentation of high-mannose N-linked glycans. *J Am Soc Mass Spectrom* 2005; 16:631-46; PMID:15862765; <http://dx.doi.org/10.1016/j.jasms.2005.01.005>
  45. Harvey D, Royle L, Radcliffe CM, Rudd PM, Dwek RA. Structural and quantitative analysis of N-linked glycans by matrix-assisted laser desorption ionization and negative ion nanospray mass spectrometry. *Anal Biochem* 2008; 376:44-60; PMID:18294950; <http://dx.doi.org/10.1016/j.ab.2008.01.025>
  46. Yu C, Crispin M, Sonnen AFP, Harvey DJ, Chang VT, Evans EJ, Scanlan CN, Stuart D, Gilbert RJC, Davis SJ. Use of the  $\alpha$ -mannosidase I inhibitor kifunensine allows the crystallization of apo CTLA-4

- homodimer produced in long-term cultures of Chinese hamster ovary cells. *Acta Cryst F* 2011; 67:785-9; PMID:21795794; <http://dx.doi.org/10.1107/S1744309111017672>
47. Maley F, Trimble RB, Tarentino AL, Plummer T, Jr. Characterization of glycoproteins and their associated oligosaccharides through the use of endoglycosidases. *Anal Biochem* 1989; 180:195-204; PMID:2510544; [http://dx.doi.org/10.1016/0003-2697\(89\)90115-2](http://dx.doi.org/10.1016/0003-2697(89)90115-2)
  48. Stover NA, Krieger CJ, Binkley G, Dong Q, Fisk DG, Nash R, Sethuraman A, Weng S, Cherry JM. *Tetrahymena* Genome Database (TGD): a new genomic resource for *Tetrahymena thermophila* research. *Nucleic Acids Res.* 2006; 34 (Database issue):D500-3; PMID:16381920; <http://dx.doi.org/10.1093/nar/gkj054>
  49. Ecker DM, Jones SD, Levine HL. The therapeutic monoclonal antibody market. *mAbs* 2015; 7:9-14; PMID:25529996; <http://dx.doi.org/10.4161/19420862.2015.989042>
  50. Zhang J. In: *Manual of Industrial Microbiology and Biotechnology*, Third Edition. Baltz RH, Demain AL, Davies JE, Bull AT, Junker B, Katz L, Lynd LR, Masarekar P, Reeves CD, Zhao H. (Editors) ASM Press, Washington, DC; 2010
  51. Frenzel A, Hust M, Schirrmann T. Expression of recombinant antibodies. *Front Immunol* 2013; 4:217; PMID:23908655; <http://dx.doi.org/10.3389/fimmu.2013.00217>
  52. Ho SCL, Tong YW, Yang Y. Generation of monoclonal antibody-producing mammalian cell lines. *Pharmaceut Bioproc* 2013; 1:71-87; <http://dx.doi.org/10.4155/pbp.13.8>
  53. Dick LW, Jr, Qui D, Mahon D, Adamo M, Cheng KC. C-terminal lysine variants in fully human monoclonal antibodies. *Biotechnol Bioeng* 2008; 100(6):1132-43; PMID:18553400; <http://dx.doi.org/10.1002/bit.21855>
  54. Jefferis R. Glycosylation of recombinant antibody therapeutics. *Biotechnol Prog* 2005; 21:11-6; PMID:15903235; <http://dx.doi.org/10.1021/bp040016j>
  55. Liu YD, Flynn GC. Effect of high mannose glycan pairing on IgG antibody clearance. *Biologicals* 2016; 44(3):163-9; PMID:26992607; <http://dx.doi.org/10.1016/j.biologicals.2016.02.003>
  56. Rustandi RR, Washabaugh MW, Wang Y. Applications of CE SDS gel in development of biopharmaceutical antibody-based products. *Electrophoresis* 2008; 29:3612-20; PMID:18803223; <http://dx.doi.org/10.1002/elps.200700958>
  57. Lux A, Yu X, Scanlan CN, Nimmerjahn F. Impact of immune complex size and glycosylation on IgG binding to human FcγRs. *J Immunol.* 2013; 190(8):4315-23; PMID:23509345; <http://dx.doi.org/10.4049/jimmunol.1200501>
  58. Baruah K, Bowden TA, Krishna BA, Dwek RA, Crispin M, Scanlan CN. Selective deactivation of serum IgG: a general strategy for the enhancement of monoclonal antibody receptor interactions. *J Mol Biol.* 2012; 420(1-2):1-7; PMID:22484364; <http://dx.doi.org/10.1016/j.jmb.2012.04.002>
  59. Preithner S, Elm S, Lippold S, Locher M, Wolf A, da Silva AJ, Baeuerle PA, Prang NS. High concentrations of therapeutic IgG1 antibodies are needed to compensate for inhibition of antibody-dependent cellular cytotoxicity by excess endogenous immunoglobulin G. *Mol Immunol.* 2006; 43(8):1183-93; PMID:16102830; <http://dx.doi.org/10.1016/j.molimm.2005.07.010>
  60. Taniguchi T, Mizuochi T, Banno Y, Nozawa Y, Kobata A. Carbohydrates of lysosomal enzymes secreted by *Tetrahymena pyriformis*. *J Biol Chem* 1985; 260:13941-6; PMID:2932444
  61. Kurz S, Tiedtke A. The Golgi apparatus of *Tetrahymena thermophila*. *J Eukaryot Microbiol* 1993; 40:10-3; PMID:8457796; <http://dx.doi.org/10.1111/j.1550-7408.1993.tb04874.x>
  62. Blum JJ. Lysosomal hydrolase secretion by *Tetrahymena*: a comparison of several intralysosomal enzymes with the isoenzymes released into the medium. *J Cell Physiol* 1976; 89:457-72; PMID:10311; <http://dx.doi.org/10.1002/jcp.1040890311>
  63. Hossler P, Khattak SF, Li ZJ. Optimal and consistent protein glycosylation in mammalian cell culture. *Glycobiology* 2009; 19:936-49; PMID:19494347; <http://dx.doi.org/10.1093/glycob/cwp079>
  64. Rouiller Y, Périlleux A, Collet N, Jordan M, Stettler M, Broly H. A high-throughput media design approach for high performance mammalian fed-batch cultures. *Mabs* 2013; 5:501-11; PMID:23563583; <http://dx.doi.org/10.4161/mabs.23942>
  65. Banno Y, Sasaki N, Nozawa Y. Secretion heterogeneity of lysosomal enzymes in *Tetrahymena pyriformis*. *Exp Cell Res* 1987; 170:259-68; PMID:2954837; [http://dx.doi.org/10.1016/0014-4827\(87\)90304-1](http://dx.doi.org/10.1016/0014-4827(87)90304-1)
  66. Krapp S, Mimura Y, Jefferis R, Huber R, Sondermann P. Structural analysis of human IgG-Fc glycoforms reveals a correlation between glycosylation and structural integrity. *J Mol Biol* 2003; 325:979-989; PMID:12527303; [http://dx.doi.org/10.1016/S0022-2836\(02\)01250-0](http://dx.doi.org/10.1016/S0022-2836(02)01250-0)
  67. Crispin M, Bowden TA, Coles CH, Harlos K, Aricescu AR, Harvey D, Stuart DI, Jones EY. Carbohydrate and domain architecture of an immature antibody glycoform exhibiting enhanced effector functions. *J Mol Biol* 2009; 387:1061-66; PMID:19236877; <http://dx.doi.org/10.1016/j.jmb.2009.02.033>
  68. Goetze AM, Liu YD, Zhang Z, Shah B, Lee E, Bondarenko PV, Flynn GC. High-mannose glycans on the Fc region of therapeutic IgG antibodies increase serum clearance in humans. *Glycobiology* 2011; 21:949-59; PMID:21421994; <http://dx.doi.org/10.1093/glycob/cwr027>
  69. Xie R, Clark KM, Gorovsky MA. Endoplasmic reticulum retention signal-dependent glycylation of the Hsp70/Grp170-related Pgp1p in *Tetrahymena*. *Eukaryot Cell* 2007; 6:388-97; PMID:17189490; <http://dx.doi.org/10.1128/EC.00366-06>
  70. Gaertig J, Kapler G. Transient and stable DNA transformation of *Tetrahymena thermophila* by electroporation. *Methods Cell Biol* 2000; 62:485-500; PMID:10503213; [http://dx.doi.org/10.1016/S0091-679X\(08\)61552-6](http://dx.doi.org/10.1016/S0091-679X(08)61552-6)
  71. Laemmli UK. Cleavage of structural proteins during the assembly of the head of bacteriophage T4. *Nature* 1970; 227:680-5; PMID:5432063; <http://dx.doi.org/10.1038/227680a0>
  72. Wang S, Ionescu R, Peekhaus N, Leung JY, Ha S, Vlasak J. Separation of post-translational modifications in monoclonal antibodies by exploiting subtle conformational changes under mildly acidic conditions. *J Chromatogr A* 2010; 1217:6496-502; PMID:20828701; <http://dx.doi.org/10.1016/j.chroma.2010.08.044>
  73. Dorion-Thibaudeau J, Raymond C, Lattová E, Perreault H, Durocher Y, De Crescenzo G. Towards the development of a surface plasmon resonance assay to evaluate the glycosylation pattern of monoclonal antibodies using the extracellular domains of CD16a and CD64. *J Immunol Methods* 2014; 408:24-34; PMID:24810583; <http://dx.doi.org/10.1016/j.jim.2014.04.010>
  74. Neville DCA, Dwek RA, Butters TD. Development of a single column method for the separation of lipid- and protein-derived oligosaccharides. *J Proteome Res* 2009; 8:681-7; PMID:19099509; <http://dx.doi.org/10.1021/pr800704t>
  75. Harvey D, Merry A, Royle L, Campbell M, Dwek RA, Rudd PM. Proposal for a standard system for drawing structural diagrams of N- and O-linked carbohydrates and related compounds. *Proteomics* 2009; 9:3796-3801; PMID:19670245; <http://dx.doi.org/10.1002/pmic.200-900096>
  76. Crispin M, Yu X, Bowden TA. Crystal structure of sialylated IgG Fc: implications for the mechanism of intravenous immunoglobulin therapy. *Proc Natl Acad Sci U S A* 2013; 110:E3544-46; PMID:23929778; <http://dx.doi.org/10.1073/pnas.1310657110>
  77. Petrescu AJ, Butters TD, Reinkensmeier G, Petrescu S, Platt FM, Dwek RA, Wormald MR. The solution NMR structure of glycosylated N-glycans involved in the early stages of glycoprotein biosynthesis and folding. *EMBO J* 1997; 16:4302-10; PMID:9250674; <http://dx.doi.org/10.1093/emboj/16.14.4302>